# The Structuring of Nonadsorbed Nanoparticles and Polyelectrolyte Chains in the Gap between a Colloidal Particle and Plate

**Martin Piech[†] and John Y. Walz***

*Yale University, Department of Chemical Engineering, P.O. Box 208286, New Haven, Connecticut 06520-8286*

*Received: January 27, 2004; In Final Form: April 14, 2004*

The force profiles between negatively charged silica and titania surfaces in solutions containing additives of either rigid spherical nanoparticles or polyelectrolyte chains, also negatively charged, were measured using an atomic force microscope (AFM). The effects of various solution conditions (e.g., additive concentration, solution ionic strength, pH) on the nature of the measured force profiles were investigated. The primary focus of the work, however, was the long-range oscillations in the force profile and the specific dependence of the wavelength of these oscillations on both solution chemistry and the bulk additive concentration. In the case when spherical nanoparticles (Ludox silica) were used as depletants, the characteristic spacing between macromolecules in the gap region followed the space-filling behavior expected of the bulk suspension (i.e., the wavelength of the oscillations in the force profile scaled with the bulk nanoparticle concentration, $c$, as $c^{-1/3}$). In addition, the actual *magnitude* of this spacing was approximately equal to $n^{-1/3}$, where $n$ is the bulk number density. For a system in which the additive was potassium polyacrylate, measurements of the force profile was made in both the dilute and semidilute regimes. Good agreement was found between the experimental and theoretical chain−chain spacing in both solution regimes, indicating that the spacing between the polyelectrolyte coils in the gap region is controlled by the bulk behavior. Specifically, the chains were space-filling in the dilute regime (i.e., the wavelength of the oscillations scaled as $c^{-1/3}$) and formed a mesh in the semidilute regime, with the wavelength of the oscillations scaling as $c^{-1/2}$. In addition, the concentration at which this change in scaling behavior occurred agreed with the expected overlap concentration.

## Introduction

The behavior of binary colloid−colloid mixtures and that of colloidal suspensions containing polymer or polyelectrolyte chains remains a subject of great interest. For example, the depletion interaction, arising from the exclusion of polymer coils or other nonadsorbing material (e.g., polyelectolyte chains, other colloidal particles, micelles, etc.) from the gap region between two colloidal surfaces, has been investigated both theoretically and experimentally by numerous authors. Fundamentally, this attraction is produced by the imbalance between the osmotic pressure in the gap region and that in the bulk arising from this difference in depletant concentration.

In addition to the purely attractive depletion force, oscillatory interactions (also referred to as structural interactions), arising from the ordering of the depletant material in the gap region at increasing depletant concentrations, have been both predicted and observed experimentally.[1−23] These oscillations are especially evident in highly charged systems (e.g., charged colloidal particles or surfaces in solution with charged nanoparticles or polyelectrolyte chains) and have been measured using a variety of experimental techniques, including total internal reflection microscopy,[11−15] atomic force microscopy,[16−21] the surface forces apparatus,[22] and an optical tweezers technique.[23]

Many of these previous studies have focused on the magnitudes of the depletion and structural components of the interaction profiles, specifically how these magnitudes vary with depletion concentration and solution chemistry (e.g., ionic strength). The aim of this current work, however, was to investigate the wavelength of the long-range oscillatory profile. Since these oscillations arise from the structuring of the depletant material in the gap, the wavelength of these oscillations should correspond to the average spacing of this material. Our specific goal was to determine the relationship between the spacing in the gap and that expected in the bulk.

Using an atomic force microscope, we measured the force curves between silica and titania surfaces in solutions containing either spherical silica nanoparticles or anionic polyacrylate (PAA) coils. The effects of depletant concentration, ionic strength, and pH on the oscillatory structure were measured.

## Experimental Section

**Reagents.** Water for preparing the solutions was produced using a NANOPure deionization system from Millipore, equipped with a 0.22 $\mu$m filter. The measured resistivity was always at least 18.2 MΩ cm. Electrolyte solutions were prepared using A.C.S.-grade $KNO_3$ (Aldrich Chemical Co., Inc., Milwaukee, WI). The solution pH was adjusted with standardized stock solutions of 0.987 N $HNO_3$ and 1.0095 N KOH, both A.C.S.-grade from Aldrich. HPLC-grade ethyl alcohol (Aldrich) was used to rinse surfaces and particle probes prior to experiments.

* Author to whom correspondence should be addressed. E-mail: john.walz@yale.edu.

[†] Current address: Sandia National Laboratories - NM, 1515 Eubank Blvd. SE, MS 1411, Albuquerque, NM 87123

10.1021/jp040067z CCC: $27.50 
Published on Web 06/03/2004

**TABLE 1: AFM Experiments with Ludox TMA Nanospheres between Silica Surfaces**

| expt # | $\phi^a$ (%) | I$^b$ (mM) | $\kappa^{-1}$ $^c$ (nm) | pH | $\xi_{exp}$ $^d$ (nm) | $\xi_{bulk}$ $^e$ (nm) | $\zeta_{paricle}$ $^f$ (mV) | $\zeta_{plate}$ $^g$ (mV) | $\zeta_{Ludox}$ $^h$ (mV) |
|---|---|---|---|---|---|---|---|---|---|
| 1 | 0.35 | 0.76 | 11.1 | 5.6 | $-^i$ | 122.6 | −82.5 | −55.2 | −67.5 |
| 2 | 1.5 | 0.76 | 11.1 | 5.6 | 73.1 ± 3.7 | 75.5 | −82.5 | −55.2 | −67.5 |
| 3 | 1.75 | 0.76 | 11.1 | 3.1 | 67.2 ± 5.9 | 71.7 | −17.0 | −24.0 | −44.0 |
| 4 | 1.75 | 0.76 | 11.1 | 4.5 | 67.4 ± 2.7 | 71.7 | −63.0 | −46.0 | −60.0 |
| 5 | 1.75 | 0.76 | 11.1 | 5.6 | 69.7 ± 5.9 | 71.7 | −82.5 | −55.2 | −67.5 |
| 6 | 1.75 | 0.76 | 11.1 | 7.0 | 69.0 ± 4.5 | 71.7 | −95.0 | −62.0 | −77.5 |
| 7 | 1.75 | 0.76 | 11.1 | 8.5 | 68.4 ± 8.1 | 71.7 | −99.0 | −64.0 | −88.0 |
| 8 | 2.5 | 0.55 | 13.2 | 5.6 | 62.3 ± 5.3 | 63.6 | −88.5 | −58.0 | −86.5 |
| 9 | 2.5 | 0.76 | 11.1 | 5.6 | 60.9 ± 4.5 | 63.6 | −82.5 | −55.2 | −67.5 |
| 10 | 2.5 | 1.5 | 7.9 | 5.6 | 59.5 ± 4.0 | 63.6 | −76.5 | −51.5 | −57.5 |
| 11 | 2.5 | 2.5 | 6.1 | 5.6 | 60.0 ± 4.3 | 63.6 | −72.0 | −47.6 | −50.0 |
| 12 | 3.5 | 0.76 | 11.1 | 5.6 | 53.9 ± 2.6 | 56.9 | −82.5 | −55.2 | −67.5 |
| 13 | 4.5 | 0.76 | 11.1 | 5.6 | 50.5 ± 2.2 | 52.3 | −82.5 | −55.2 | −67.5 |

[a] The silica nanosphere volume fraction. [b] The "effective" ionic strength accounting for both the added electrolyte and the counterions released from the nanospheres. [c] Solution Debye length calculated from the known ionic strength. [d] The period of structural oscillations in the experimental force profile; the reported variability represents standard deviation whenever more than 4 measurements were available. [e] The average spacing between nanospheres in the bulk suspension calculated using eq 2. [f] The $\zeta$-potential of 5 $\mu$m diameter silica spheres determined with a Rank Brothers MKII microelectrophoresis apparatus. [g] The streaming potential of a silica plate measured using an asymmetric clamping cell (Anton Paar, Graz, Austria, see ref 26) attached to a commercial streaming potential analyzer (EKA, Brookhaven Instruments, Holtsville, NY). [h] The $\zeta$-potential of Ludox TMA colloidal silica measured using an electroacoustic spectrometer (model DT-1200 from Dispersion Technologies, Inc., Mount Kisco, NY). [i] No structural oscillations were detected in the measured force profile.

**Colloidal Probes.** The AFM "colloidal probes" were prepared by gluing either silica spheres (3 $\mu$m and 5 $\mu$m diameter particles from Bangs Laboratories Inc., Fishers, IN) or hollow titania spheres (1−2.5 $\mu$m particles synthesized[24] and donated by Stefanie Eiden from the University of Konstanz, Konstanz, Germany) to the tips of AFM cantilevers (Bio-levers from Asylum Research Corporation, Santa Barbara, CA) using a UV-curable epoxy (NEA 123L adhesive from Norland Product Inc., Cranbury, NJ). Exposure of the probes to UV radiation prior to an experiment had the dual effect of curing the glue and removing organic contamination. Imaging with scanning electron microscopy (SEM) and AFM showed both types of particles to be highly spherical with relatively smooth surfaces (mean surface roughness, $R_a$, determined over a 0.5 × 0.5 $\mu$m area was 1.2 and 2.6 nm for the silica and titania colloids, respectively).

Electrophoretic mobilities of silica and titania colloids from the same batch as the test particles used in fabricating the AFM probes were measured using microelectrophoresis (Model MKII, Rank Brothers Ltd., Cambridge, UK). The measured mobilities were converted to $\zeta$ potentials ($\zeta_{particle}$) using the program of O'Brien and White.[25] Some example values of $\zeta_{particle}$ for the 5 $\mu$m diameter silica particles at various experimental conditions are given in Table 1.

**Surfaces.** Two types of silica surfaces were used in the experiments: (1) polished silica flats (Melles Griot, Irvine, CA) with $R_a$ = 0.65 nm (measured over a 1 $\mu$m × 1 $\mu$m area), and (2) an oxidized silicon wafer with $R_a$ = 0.12 nm over the same area. This latter sample was prepared by exposing an Si(111) substrate (prime class wafer from Silicon Electro-Physics, Inc., Bradford, PA) to ultrahigh purity $O_2$ (Airgas, Inc., Radnor, PA) at 950 °C for 1 h, followed by quenching with water vapor. Samples were cleaned with ethanol, treated with an $H_2SO_4$/Nochromix oxidizing solution (GODAX Laboratories, Inc., Takoma Park, MD), sonicated, and thoroughly rinsed in deionized (DI) water. Titanium dioxide samples were polished rutile(110) single-crystal sheets from Princeton Scientific Corporation (Princeton, NJ), characterized by $R_a$ = 0.19 nm over a 1 $\mu$m × 1 $\mu$m area. Cleaning was accomplished by overnite soaking in 1 mM $HNO_3$ solution, followed by steam treatment with DI water for ≈3 h. After drying with high-purity filtered argon (Airgas, Inc., Radnor, PA), all surfaces were exposed to UV/$O_3$ treatment (TipCleaner from BioForce Nanosciences, Inc., Arnes, IA) for approximately 45 min and immediately mounted into the AFM fluid cell.

The silica plate streaming potential ($\zeta_{plate}$) was measured with a new asymmetric clamping cell (Anton Paar, Graz, Austria)[26] attached to a commercial streaming potential analyzer (EKA, Brookhaven Instruments, Holtsville, NY). To within experimental error, measurements carried out on the Melles Griot substrate were the same as those performed with the oxidized silicon wafer. The silica plates were found to be negatively charged for all test conditions. Some example values of $\zeta_{plate}$ for the Melles Griot silica surface are given in Table 1. Due to the limited size of the single-crystal rutile sheets, it was not possible to measure the streaming potential of these substrates.

**Depletants.** Two different depletant species were employed in this study: (1) charged, rigid nanospherical particles, and (2) semi-flexible polyelectrolyte chains. In the first case, Ludox grade TMA colloidal silica was used. It was obtained from Aldrich as a 34 wt % aqueous dispersion in deionized water. The nanoparticles were contacted with a clean, mixed bed of biotechnology grade resin (AG 501-X8 (D) from Bio-Rad Laboratories, Hercules, CA) for a period of 12 h to remove any remaining ions and ionic contaminants (the resin was cleaned with several rinses of DI water and ethanol).

The manufacturer reported the diameter of these nanospheres to be 22 nm. Using similar silica particles (Ludox AS-40 grade), Blaaderen and Kentgens measured the actual diameter to be 22.2 ± 4.4 nm compared to the manufacturer quoted value of 22 nm.[27] Here, the size of Ludox TMA particles was measured with photon correlation spectroscopy (PCS) of quasi-elastically scattered light (QELS) utilizing a Brookhaven ZetaPlus instrument (Brookhaven Instruments Corporation, Holtsville, NY) with multiangle sizing option. The intensity-weighted average diameter, $d_{intens}$, obtained from this measurement was 32 nm. Assuming a log−normal distribution[3,28] of particle diameters with the standard deviation taken to be the value given in the literature,[27] this $d_{intens}$ value was converted to the number-average diameter, $d$ = 26 nm. (It should be mentioned that assuming a normal distribution instead did not significantly alter the results.) Because PCS yields a hydrodynamic diameter, the measurements are expected to slightly overestimate the manufacturer-reported sizes, which were obtained with transmission electron microscopy (TEM).

$\zeta$-Potentials of the Ludox nanospheres ($\zeta_{Ludox}$) were determined at the same conditions employed in the AFM experiments using an electroacoustic spectrometer (model DT-1200 from Dispersion Technologies, Inc., Mount Kisco, NY) equipped with an automatic titrator. The $\zeta_{Ludox}$ values were all negative and some examples are given in Table 1. Unfortunately, due to the limited number of measurements (e.g., typically 2−3) at each set of conditions, the variability of the measured $\zeta$-potentials could not be reliably estimated. In the few cases when a larger number of data points was acquired (ca. 10−12), the standard deviation was found to be on the order of 7% of the mean, indicating good reproducibility.

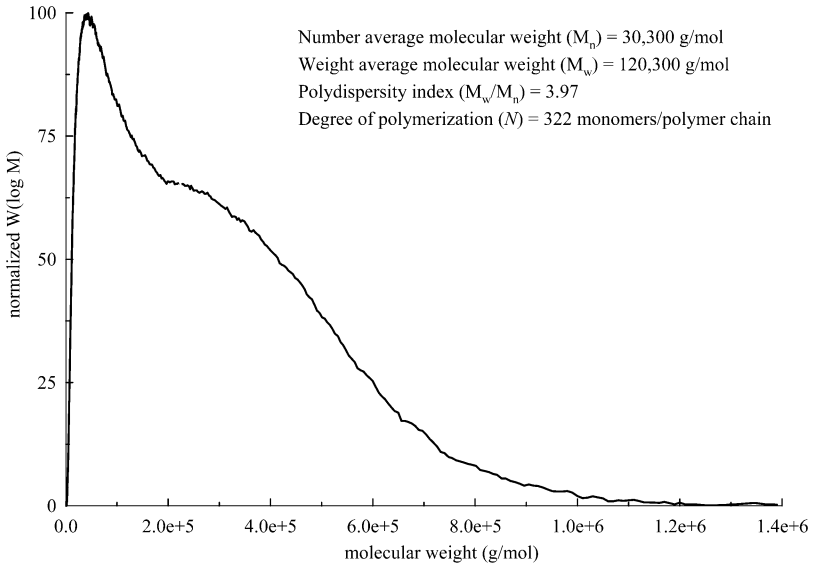


**Figure 1.** Molecular weight distribution of the polyacrylate sample used here, determined by gel permeation/size exclusion chromatography (GPC/SEC). Note that the measurements were made using sodium polyacrylate instead of potassium polyacrylate.

In the experiments with semi-flexible polyelectrolyte depletants, potassium polyacrylate (KPAA) chains were used. The KPAA samples were obtained by diluting commercially available poly(acrylic acid) solution (Aldrich) and titrating with KOH until a pH value of 8−8.5 was obtained. Prior to the titration, the initial acidic material was dialyzed against deionized water for a period of 10 days, with the water changed every day. Next, the dialyzed PAAH was contacted with a clean, mixed bed of biotechnology grade resin as described above. Finally, the appropriately diluted solutions were titrated in a gas-tight Teflon vessel pre-purged with argon to minimize $CO_2$ contamination.

The manufacturer quoted the molecular weight of the poly(acrylic acid) sample used here to be 100 000 g/mol. To determine the molecular weight distribution of the cleaned material (i.e., after dialysis and deionization, but before titration), gel permeation/size exclusion chromatography (GPC/SEC) was performed. The PAAH samples were first converted to the corresponding sodium salts (this was done because the calibration standards were available in the NaPAA form) and then passed through a series of two mixed PL-aquagel-OH columns, followed by a PL-aquagel-OH 30 column (both from Polymer Laboratories Inc., Amherst, MA) with aqueous 0.2 M $NaNO_3$ solution containing 20% vol of methanol used as the eluent phase. The instrument was calibrated with NaPAA standards (i.e., $M_w$ = 1930; 8300; 83,400; and 245,200 g/mol from American Polymer Standards Corp., Mentor, OH). The measured polymer molecular weight distribution shown in Figure 1. The GPC/SEC analysis results are also summarized in the figure. As can be seen, the sample is highly polydisperse (it is also bidisperse) with the MW distribution exhibiting a strong positive skewing.

**Depletant Suspensions.** All depletant suspensions utilized in the AFM experiments and characterization work were prepared in a gas-tight Teflon vessel pre-purged with argon to minimize $CO_2$ contamination. After diluting an appropriate amount of the macromolecule stock solution with DI water, the suspension pH and ionic strength were adjusted by titrating with $HNO_3$, KOH, or $KNO_3$ solutions of a known molarity. The suspension conductivity, pH, and temperature were continuously monitored employing suitable sensors within the vessel. These measurements, along with the known ionic mobilities of the ions in the system, were then used to calculate the solution ionic strength.

The concentration of depletant material was determined by drying a known amount of suspension. In the case of silica nanoparticles, the weight fraction obtained in this manner was then converted to the volume fraction using the known density, $\rho_{SiO_2} = 2.37$ g/cm$^3$. This value was calculated on the basis of the mass of a known volume of the suspension before and after drying at 400 °C for 24 h.

**AFM Force Measurements.** A Nanoscope Multimode AFM (Digital Instruments Ltd., Santa Barbara, CA) equipped with a fluid cell was used to measure the force−distance profiles between the silica or titania surfaces. The protocol of Ducker et al.[29] was utilized to convert the raw data into force−separation plots. All measurements were performed with 100 $\mu$m rectangular cantilevers (Bio-levers) having a nominal spring constant of $6 \times 10^{-3}$ N/m. Each cantilever spring constant was calibrated individually using the method of Sader et al.,[30] which yielded values between $(3.4 \pm 0.5) \times 10^{-3}$ N/m and $(6.2 \pm 0.5) \times 10^{-3}$ N/m (these uncertainties are 95% confidence intervals). Scanning frequencies were varied from 0.05 to 0.3 Hz over a scan size of 250−300 nm, which corresponded to approach velocities in the range 12.5−90 nm/s. Chan and Horn[31] showed that hydrodynamic drainage forces are negligible at these approach speeds. In addition, several long-range scans (1−2 $\mu$m) were acquired to capture a larger portion of the linear region in the force curve and to ensure that the force curve baseline was free from optical interference artifacts.

The standard procedure in AFM force measurements for determining the point of zero separation is to determine the point at which the cantilever deflection becomes linearly related to the scanner movement (termed constant compliance).[29] Because of the low spring constant of the cantilevers used in these experiment, in conjunction with the strong electrostatic repulsive force between the particle and substrate, this point would seemingly be reached before hard contact was ever achieved. As a result, determination of the absolute separation distance was not possible. Nonetheless, the *relative* separation between different parts of a given force profile is accurate, as is the measured value of the force.

Prior to each experiment, the cell was thoroughly rinsed with ethanol and DI water. The test solution was introduced shortly afterward and allowed to equilibrate for 30 min (longer equilibration times did not alter the force−distance data).

During each experiment, between 40 and 60 force-vs-distance profiles were typically recorded, which were then averaged together to obtain the final curve. Only those curves with a flat baseline and a minimum amount of noise were selected. The averaging procedure consisted of first separating all of the measured data into bins ranging between 0.4 and 4 nm (the bin width was adjusted to give 200 data points per bin), and then calculating the mean and 95% confidence interval for the data in each bin. The 95% confidence limits were typically found to range between 0.2 and 0.35 pN.

Following a series of force measurements, the AFM probes were inspected visually to make sure that the colloidal particles had not fallen off. Last, at the end of its service, each cantilever probe was imaged with a scanning electron microscope (Amray 1920 ECO SEM from Amray Inc., Bedford, MA) to determine the cantilever dimensions (its length, $l$, and width, $b$), the particle radius, $R$, and the particle placement, $\Delta l$. At this point the spring constant was recalculated using the measured values of $l$ and $b$ and corrected for the sphere placement as described by Sader et al.[32] The accurate determination of colloidal particle size also facilitated direct comparison between experiments carried out with different AFM probes by scaling the measured force by $R$. Furthermore, if the particle surface was contaminated by glue or other debris near its apex (i.e., the area expected to make contact with the sample), the collected data set was disregarded and the measurements repeated.

## Results and Discussion

**Experiments with Spherical Silica Nanoparticles.** The experiments performed here measured the force of interaction between a silica or titania colloid attached to an AFM cantilever and a flat silica or titania surface in solutions containing spherical silica nanoparticles (Ludox TMA colloidal silica). Because the measurements were performed at pH greater than 5.5, all surfaces were negatively charged, which created repulsive electrostatic interactions between all species in the suspension (i.e., the silica and titania colloids/surfaces and the silica nanospheres). Upon approach of the colloidal probe and the flat substrate, the total force between these surfaces, $F_{tot,sp}(h)$, was a summation of the repulsive electrostatic double-layer force, $F_{el}(h)$, the attractive van der Waals force, $F_{vdW}(h)$, and the depletion force, $F_{dep,sp}(h)$. (Note that $F_{dep,sp}(h)$ is assumed to represent both the attractive and longer range oscillatory components of the force.)

$$F_{tot,sp}(h) = F_{el}(h) + F_{vdW}(h) + F_{dep,sp}(h) \qquad (1)$$

Shown in Figure 2 is a measured force profile for a 4.45 $\mu$m diameter silica sphere interacting with an oxidized silicon wafer in a suspension of silica nanospheres at varying volume fractions of added nanospheres. The solution ionic strength and pH were adjusted to 0.76 mM and 5.6, respectively, while other system parameters are listed in the figure caption. A summary of the conditions used in each experiment is given in Table 1.

As explained in the Experimental section, the gap between the two surfaces could only be estimated and is reported as "relative separation". Nonetheless, the separation distance between features in a given force profile is accurate, as is the value of the force itself (notice that the force is scaled by the colloidal particle radius to allow direct comparison between different experiments).

*The Effect of Nanoparticle Concentration.* At the lowest nanosphere volume fraction of 0.35% (Figure 2a) only the attractive component of the depletion force can be detected, in addition to the strong electrostatic repulsion at smaller separations (the attractive van der Waals interaction becomes significant only at much lower gap widths). Meanwhile, for larger volume fractions (Figure 2b and 2c), the oscillatory interaction is also present at larger separations. These force oscillations can be attributed to the mutual repulsion between the nanospheres, leading to their structuring in the gap.[2,4,6,7,12] As can be seen from the figure, with increasing concentration of the nanoparticles the oscillatory wavelength, $\xi_{exp}$, decreases. This parameter is defined as the separation distance between successive force minima or maxima observed in the measured force profile. The values that are reported here are the average values measured over all maxima and minima in a given force profile. It should be noted that in a given force profile, the values of this spacing did not vary significantly between the various minima and maxima (e.g., the spacing between the first two maxima was approximately equal to that between the last two maxima).

At the same time, the oscillations increase in magnitude (i.e., increasing amplitude), presumably because the nanospheres are forced closer to each other at the higher concentrations and thus encounter stronger electrostatic repulsion. Similar oscillatory interaction profiles due to charged spherical nanoparticles were reported by Piech and Walz[21] and Sharma and Walz.[12] In this latter study, the technique of total internal reflection microscopy (TIRM) was employed to measure the interaction energy between a colloidal particle undergoing Brownian motion and a flat plate. Using a line optical tweezer technique, Yodh and co-workers[23] also measured oscillatory interaction potentials between two isolated 1.1 $\mu$m diameter polymethylacrylate (PMMA) spheres induced by a background of smaller, 83 nm diameter polystyrene (PS) spheres. The bare interaction between the individual large or small particles was a screened electrostatic repulsion with a 3 nm screening length. In a related set of experiments, Wasan and co-workers[7−10] studied a stepwise draining of thin films containing nearly monodispersed, submicrometer particle suspensions of repulsive PS lattices and silica hydrosols. Not only did these authors detect stepwise pressure variations upon the film draining, but the determined height of these step-transitions was on the order of the colloidal particle diameter.

In general, all force profiles observed here were characterized by strong electrostatic repulsion at small gap widths followed by depletion attraction and longer-range structural oscillations. The oscillatory wavelength, $\xi_{exp}$, was measured whenever possible (i.e., given at least two minima in the experimental force profile) and is reported in Table 1. Also given here is the expected spacing between silica nanospheres in the bulk solution, $\xi_{bulk}$, which was calculated from the known nanoparticle size distribution, $f(a)$, and volume fraction in the suspension, $\phi$, according to

$$\xi_{bulk} = n^{-1/3} = (\phi / \int_0^\infty (4/3)\pi a^3 f(a)\, da)^{-1/3} \qquad (2)$$

where $n$ denotes the nanoparticle bulk number density, while $f(a)$ was approximated by a log−normal distribution with a mean radius of 11.0 nm and a standard deviation equal to 2.3 nm (see Experimental section). Note that this expression ignores a numerical prefactor characterizing the type of packing, which

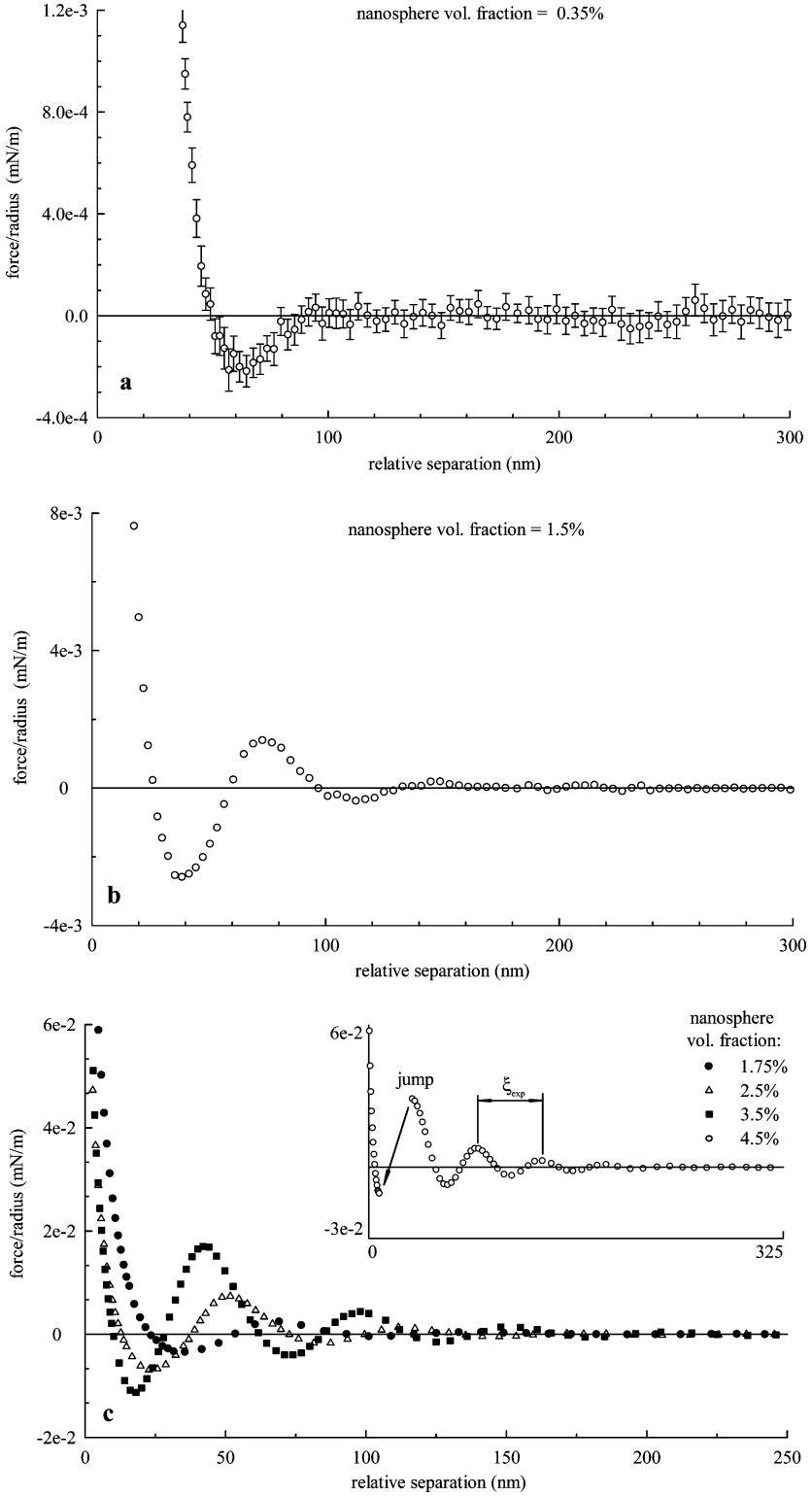


**Figure 2.** Depletion interaction between an oxidized silicon wafer and a 4.45 $\mu$m diameter silica colloid attached to a cantilever spring having $k_{spr}$ = 0.0053 N/m in a suspension of Ludox TMA nanospheres. The nanosphere volume fraction, $\phi$, was varied, while the solution pH and ionic strength were held fixed at 5.6 and 0.76 mM, respectively. (a) $\phi$ = 0.35%. The vertical error bars correspond to the 95% confidence intervals. (b) $\phi$ = 1.5%. Here the error bars are indistinguishable from the symbols. (c) $\phi$ = 1.75 to 4.5%. The insert shows the force profile at $\phi$ = 4.5%. Additionally, a cantilever "jump" to the first depletion minimum is indicated with an arrow. At that point, the gradient of the attractive depletion force exceeded the cantilever spring constant, giving rise to the observed mechanical instability. The oscillatory period, denoted by $\xi_{exp}$, is also shown in the insert.

will be of order one. It should be emphasized that $\xi_{bulk}$, which is the average separation distance between nanoparticles in the bulk, depends solely on the bulk number density and is not a function of the nanoparticle size or the double-layer thickness.

As can be seen from Table 1, the $\xi_{exp}$ values are very similar to $\xi_{bulk}$ for each experiment, with $\xi_{exp}$ smaller than $\xi_{bulk}$ by 4.5% on average (the largest deviation was equal to 6.4%). This indicates that the structure in the gap region follows the bulk

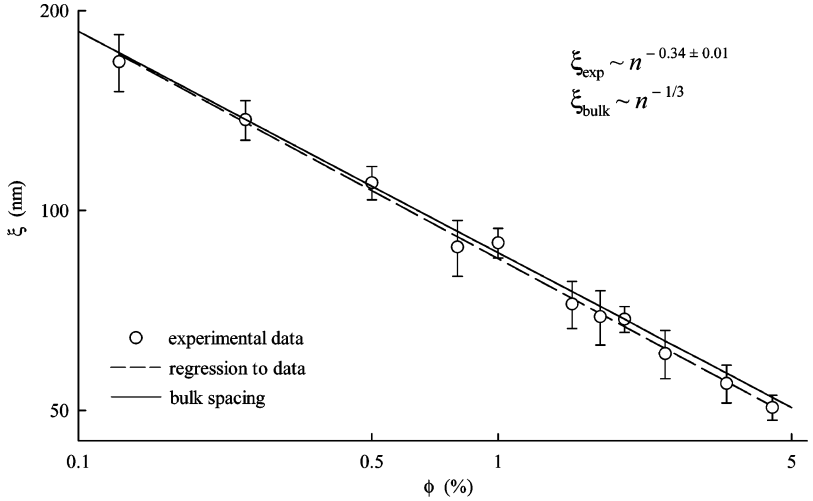


**Figure 3.** Graph illustrating the effect of macromolecule concentration, $\phi$, on the oscillatory period, $\xi_{exp}$, corresponding to the nanosphere−nanosphere spacing. Note that data are plotted on a log−log scale and the vertical error bars represent the measurement standard deviation. The solid line is a theoretical prediction of the correlation length ($\xi_{bulk}$) in the bulk suspension calculated using eq 2. As seen, the nanoparticle spacing in the gap region clearly agrees with that expected in the bulk solution. Note that the symbol $n$ in the scaling expressions given above denotes the nanoparticle number density. However, these scaling relations will be identical whether number density ($n$) or volume fraction ($\phi$) is used to express the nanoparticle concentration, since $n \propto \phi$.

suspension behavior under all conditions investigated. Figure 3 illustrates this more clearly, with $\xi_{exp}$ values plotted against the nanoparticle volume fraction on a log−log scale. Apart from the data listed in Table 1, several other experiments with titania and silica surfaces in the presence of the silica nanospheres at various solution conditions (i.e., different pH, ionic strength) were used in constructing this graph. In all cases, the force profiles were very similar to those presented in Figure 1 and were used to extract the oscillatory wavelength, $\xi_{exp}$. Also shown in Figure 3 is the best fit through the data (broken line) and the expected bulk suspension behavior calculated with eq 2 (solid line). The slope of the broken line, which is the measured scaling of the wavelength with bulk concentration, was $-0.34 \pm 0.01$, which agrees very well with the purely space filling value of $-1/3$.

From Figure 3 and Table 1, it is apparent that the measured $\xi_{exp}$ values fall within the standard deviation of the predicted $\xi_{bulk}$. However, the bulk nanoparticle spacing is typically greater than the measured spacing in the gap (as mentioned above, on average $\xi_{bulk}$ exceeds $\xi_{exp}$ by 4.5%). The use of a relatively high Ludox silica density (i.e., $\rho_{SiO_2} = 2.37$ g/cm$^3$; see Experimental section) in calculating the nonosphere volume fraction can partially explain this trend. If the lower value of $\rho_{SiO_2} = 2.286$ g/cm$^3$ estimated from the literature data[33−36] for a similar Ludox silica grade was used instead, the discrepancy between the measured $\xi_{exp}$ and the calculated $\xi_{bulk}$ would drop to approximately 1%.

These results are in qualitative agreement with recent Monte Carlo simulation by Jönsson et al.[37] These authors calculated the pressure profile acting between two hard walls in a solution that contained either point charged particles (macroions) or a flexible polyelectrolyte chain. An oscillatory pressure profile was predicted in both cases, and for the point charge model, the period of the oscillations was observed to scale as $c_{bulk}^{-1/3}$, where $c_{bulk}$ is the bulk concentration of macroions.

*The Effect of Suspension Ionic Strength.* The effect of increasing suspension ionic strength on the depletion and structural interactions is illustrated in Figure 4 for the case of silica surfaces at pH = 5.6 and constant Ludox volume fraction, $\phi = 2.5\%$ (i.e., experiments 8−11 in Table 1). It should be mentioned that these experiments were also performed using titania surfaces and very similar results were obtained, thus only the silica−silica results will be presented here.

It is clear from Figure 4a that increasing the ionic strength greatly dampens the *amplitude* of structural oscillations. At the same time, the oscillatory *wavelength* remains approximately constant, as can be seen from the results presented in Table 1 and illustrated in Figure 4b. The reduction in the magnitude of the structural force follows directly from the fact that the addition of salt significantly weakens the nanosphere−nanosphere electrostatic interactions.

Another interesting aspect of the data is the surprisingly large reduction in the structural force upon addition of only 0.21 mM $KNO_3$ to the $I = 0.55$ mM suspension. This clearly highlights the need for precise control of the ionic strength in these types of experiments. In particular, small amounts of ionic contaminants (e.g., $HCO_3^-$ from atmospheric $CO_2$) have the potential to significantly affect the measurement results.

*The Effect of Suspension pH.* The effect of increasing solution pH on depletion and structural interactions is shown in Figure 5 for the case of silica surfaces at ionic strength of 0.76 mM and constant Ludox volume fraction, $\phi = 1.75\%$. Other systems parameters are reported in the Figure 5 caption, while Table 1 lists the appropriate experiments.

As can be seen from Figure 5a, the *magnitudes* of the successive minima and maxima in the force profile vary rather weakly for the pH changes considered here. This comes from the fact that silica nanosphere−nanosphere interactions are not greatly altered. While the Ludox $\zeta$-potential changes from $-88$ mV at pH = 8−8.5 to $-44$ mV at pH = 3.1 (see Table 1), the electrostatic repulsion between the nanoparticles remains relatively strong, leading to the observed structuring in the gap. Moreover, the oscillation wavelength also remains relatively constant (see data in Table 1 and Figure 5b).

**Experiments with Polyelectrolyte Macromolecules.** Force measurements were also obtained between silica and titania surfaces in the presence of potassium polyacrylate (KPAA). The choice of materials and the types of experiments were motivated by the widespread use of polyacrylates as steric stabilizers in metal oxide dispersions.

Because all of the experiments were carried out at pH = 8−8.5, the titania and silica surfaces, as well as the dissociated

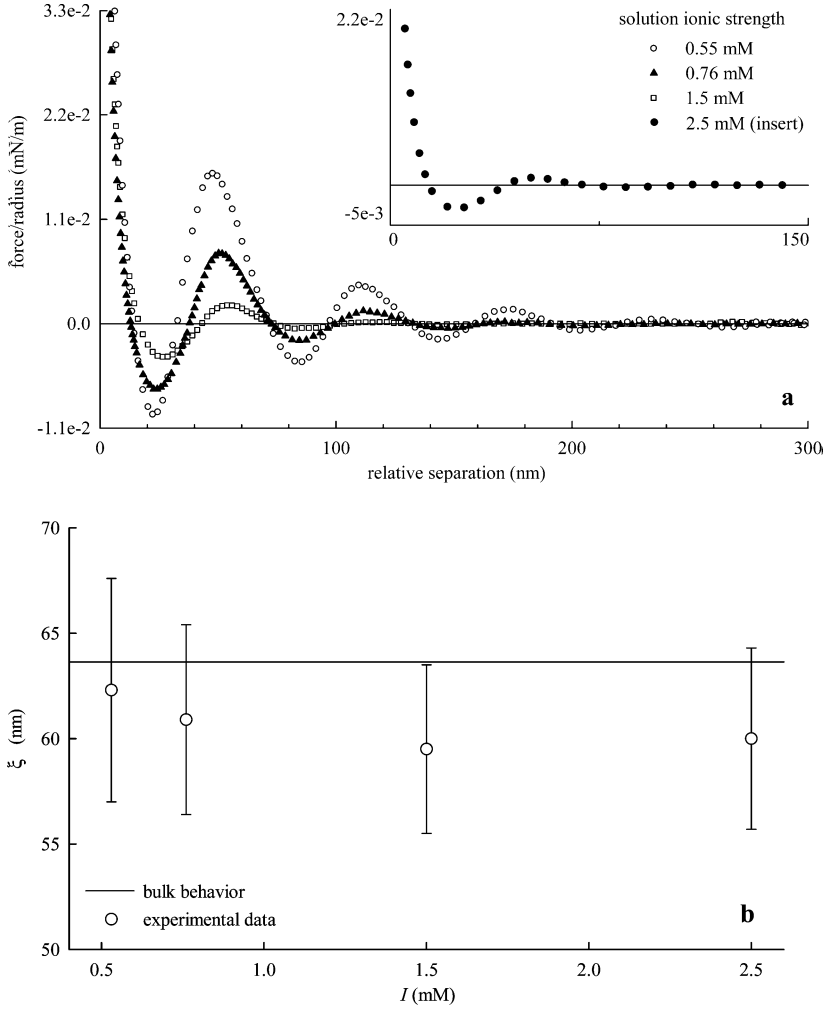


**Figure 4.** Depletion interaction between an oxidized silicon wafer and a 4.45 $\mu$m diameter silica colloid attached to a cantilever spring having $k_{spr}$ = 0.0053 N/m in a suspension of Ludox TMA nanospheres at a volume fraction, $\phi$ = 2.5%. The solution ionic strength was varied at a constant pH = 5.6. In the case of $I$ = 0.55 mM data, only $K^+$ counterions were present in suspension with no extra $KNO_3$. For all other experiments, $KNO_3$ was added to increase the solution ionic strength as specified in the graph. (a) Experimental force curves. (b) Variation of the oscillatory period with the solution ionic strength.

PAA chains, were all negatively charged and thus repulsive. Analogous to the case of the silica nanosphere depletants, the force profiles exhibited a strong electrostatic repulsion at small gap widths, followed by a depletion attraction and oscillatory structural interaction at larger separations. This is illustrated in Figure 6 for the interaction between a silica surface and a 3.0 $\mu$m diameter silica colloid in pH = 8−8.5 solution of KPAA chains at increasing concentration. The measurements were carried out under "salt-free" conditions, meaning that apart from the KOH needed to adjust the solution pH, no extra salt was added. Similar to the case of spherical Ludox depletants, raising the concentration of KPAA chains resulted in an increased amplitude and decreased wavelength of the structural oscillations in the force profiles (compare Figures 2 and 6). Moreover, at higher polyelectrolyte concentrations, the short-range electrostatic repulsion occurred at smaller gap widths. This is not surprising, since the larger number of KPAA chains produces a greater number of $K^+$ counterions and therefore a shorter Debye screening length, which determines the range of the electrostatic interaction between the AFM probe and the surface. Similar experiments with titania surfaces and a mixed system consisting of a titania AFM probe and a silica surface yielded results almost identical to the force profiles shown in Figure 6 for the silica−silica case. Table 2 reports the specific conditions for all these experiments along with oscillatory wavelength determined from the measured force profiles ($\xi_{exp}$).

It is worthwhile to note here that other researchers reported very similar interaction profiles for silica surfaces in polyelectrolyte solutions.[13−17] Specifically, the common feature of these investigations carried out with NaPAA (sodium polyacrylate[17]) and NaPSS (sodium polystyrene sulfonate[13−16]) polyelectrolytes employing either the AFM[16,17] or TIRM[13−15] techniques was the presence of short-range electrostatic repulsion and a longer-range oscillatory interaction. Similarly, Langevin and coworkers[38−40] observed stepwise thinning of films comprised of polyelectrolyte and surfactant mixtures (either NaPSS, random block copolymer: acrylamide−acrylamidesulfonate, or a random copolymer of acylamide and acrylamido-methyl-propane sulfonate in solution with dodecyltrimethylammonium bromide). The pressure oscillations observed by these authors indicated the presence of an oscillatory structural interaction between the film surfaces and were related to a network of polymer chains in the film bulk.

*Scaling Behavior of Polyelectrolyte Solutions.* In a salt-free, dilute solution, polyelectolyte molecules assume an extended conformation due to Coulombic repulsion between nearest-neighbor functional groups along the chain.[41,42] This gives rise to the stiffened "rigid rod" picture of the polyelectrolyte

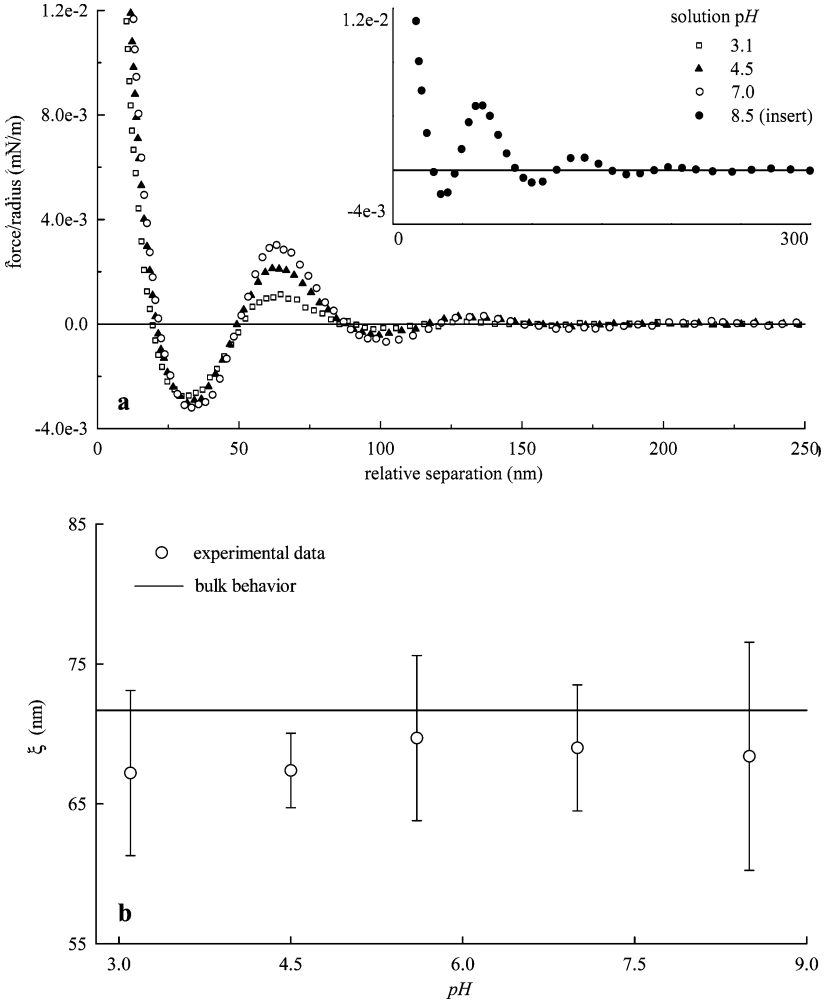


**Figure 5.** Depletion interaction between an oxidized silicon wafer and a 4.45 $\mu$m diameter silica colloid attached to a cantilever spring having $k_{spr}$ = 0.0053 N/m in a suspension of Ludox TMA nanospheres at a volume fraction, $\phi$ = 1.75%. The solution pH was varied at a constant ionic strength of 0.76 mM. (a) Experimental force curves. (b) Variation of the oscillatory period with the solution pH.

molecule. As shown by computer simulations of Stevens and Kramer,[43,44] however, full extension of the chain is very unlikely and the molecule is better described by a network of electrostatic blobs. Inside each blob, chain statistics are determined by the thermodynamic interaction between uncharged polymer and solvent, with the macromolecule conformation unperturbed by the electrostatic interactions. On the length scale of the entire polyelectrolyte molecule, the blobs form an extended (rodlike) configuration determined by electrostatic interactions. Assuming that water is a good solvent for the acrylate backbone,[17] the macromolecule chain length, $L$, can be calculated from[45]

$$L \approx Nb\left(\frac{u}{A^2}\right)^{2/7} \quad \text{for } T \gg \theta \tag{3}$$

and

$$u = l_B/b \tag{4}$$

where $N$ is the degree of chain polymerization (i.e., number of monomers), $b$ represents the monomer size, $A$ is the number of monomers between charges along the chain (assuming monovalent charges and counterions, the total charge on a chain is $N/A$), and $\theta$ denotes the polymer $\theta$ temperature. The Bjerrum length, $l_B = e^2/(\epsilon_0\epsilon_r kT)$, is the distance at which the energy of Coulombic interaction between two elementary charges is equal to the thermal energy $kT$.[46]

In dilute solutions, where the chains behave as individual macromolecules (i.e., rods of length $L$), the separation distance between them ($R_{cm}$) defines the characteristic length scale in the system ($\xi_{bulk}$). Thus

$$\xi_{bulk} = R_{cm} = \left(\frac{1}{n_{coil}}\right)^{1/3} = \left(\frac{N}{n}\right)^{1/3} \quad \text{for } n < n^* \tag{5}$$

where $n_{coil}$ and $n$ represent the number concentration of polymer coils and monomers, respectively, while $n^*$ is the overlap concentration approximated by

$$n^* \approx \frac{N}{L^3} \tag{6}$$

The overlap concentration defines the onset of the salt-free, semidilute regime, occurring just when the precessional volumes of polyelectrolyte rods begin to overlap (i.e., $R_{cm} \approx L$).

Above $n^*$, a polymer solution is characterized by the existence of a network with a specific "mesh size" $\xi_{bulk}$ (also referred to as the "correlation length"). This correlation length is on the order of the dilute solution chain size ($L$) at $n^*$ and follows a power law concentration dependence for $n > n^*$[47] with the form

$$\xi_{bulk} \approx L(n/n^*)^m \quad \text{for } n > n^* \tag{7}$$

The value of $m$ in eq 7 has been shown to equal $-1/2$ for

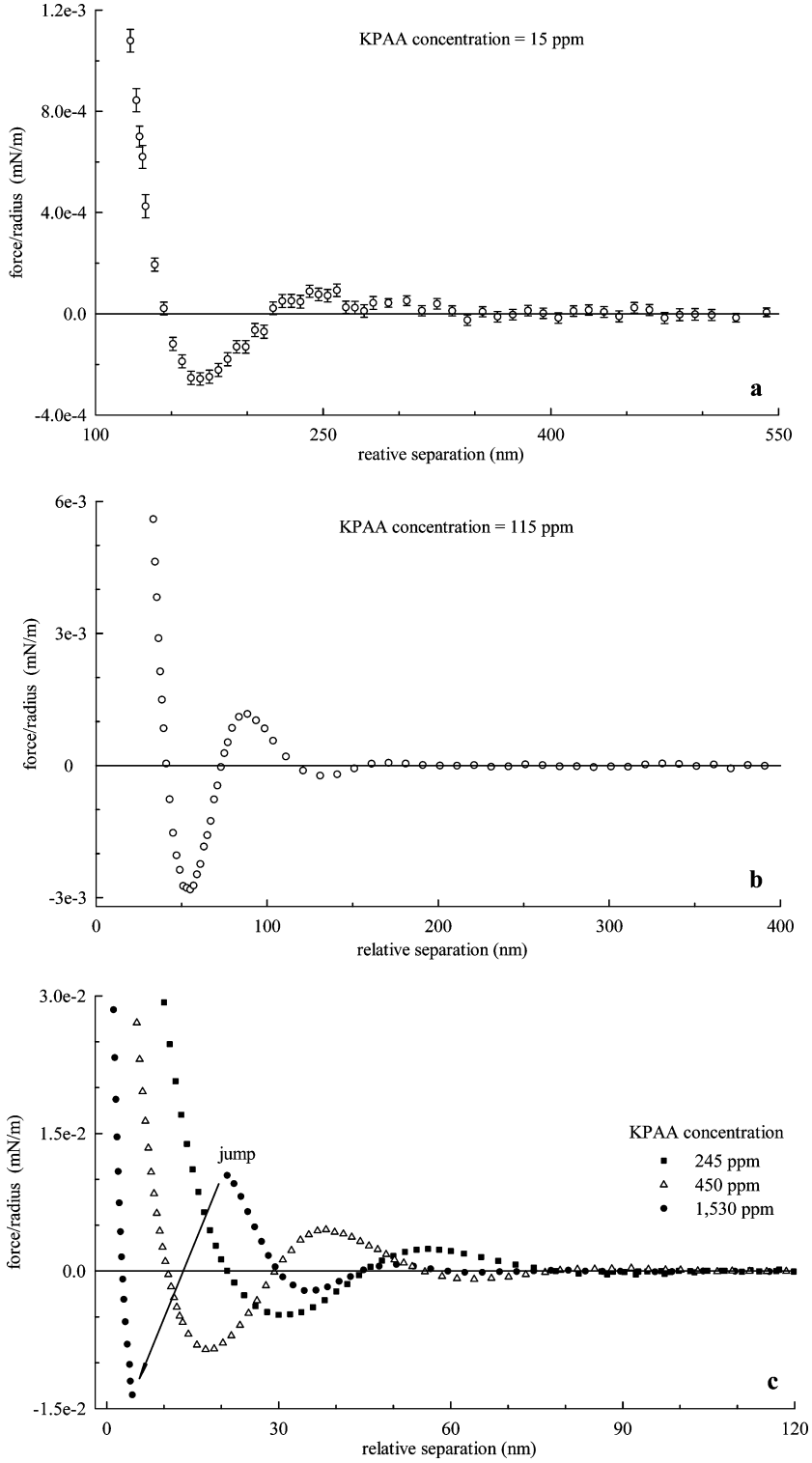


**Figure 6.** Depletion interaction between a 3.0 $\mu$m diameter silica colloid attached to a cantilever spring having $k_{spr} = 0.0034$ N/m and a Melles Griot silica substrate as a function of KPAA concentration ($c$). The solution pH was adjusted to 8−8.5 using KOH, and no extra salt was added (i.e., salt-free conditions). (a**)** $c = 15$ ppm. The vertical error bars correspond to 95% confidence intervals. (b) $c = 115$ ppm. Here the error bars are indistinguishable from the symbols. (c) $c = 245$ ppm to 1530. The cantilever "jump" to the first depletion minimum is indicated with an arrow. At that point, the gradient of the attractive depletion force exceeded the cantilever spring constant giving rise to the observed mechanical instability. Note the difference in axes scaling between graphs (a), (b), and (c).

polyelectrolytes. Thus

$$\xi_{bulk} \approx \left(\frac{B}{nb}\right)^{1/2} \text{ for } n > n^* \tag{8}$$

where $B$ represents the ratio of the chain contour length to its extended size

$$B = \frac{Nb}{L} \tag{9}$$

While in the semidilute regime, polymer coils overlap and form a network (mesh), a significant overlap is required for them to topologically constrain each other's motion (criterion for entanglement). In the case of neutral polymers, the entanglement

**TABLE 2: AFM Experiments with Titania and Silica Surfaces in pH = 8−8.5 Solutions Containing KPAA Polyelectrolyte**

| expt. no. | $c^a$ (ppm) | $I^b$ (mM) | $\xi_{exp}{}^c$ (nm) | $\xi_{bulk}{}^d$ (nm) |
|---|---|---|---|---|
| Experiments with Silica Surfaces | | | | |
| 1s | 15[e] | 0.07 | −[g] | 156.7 |
| 2s | 31[e] | 0.10 | −[g] | 124.4 |
| 3s | 61[e] | 0.16 | 99 ± 10 | 98.7 |
| 4s | 115[e] | 0.24 | 80 ± 6 | 80.1 |
| 5s | 245[e] | 0.50 | 61.5 ± 6.5 | 62.1 |
| 6s | 450[e] | 0.90 | 49 ± 4 | 50.7 |
| 7s | 910[f] | 1.70 | 39.5 ± 2.5 | 36.3 |
| 8s | 1530[f] | 2.85 | 28.5 ± 1.5 | 28 |
| Experiments with Titania Surfaces | | | | |
| 1t | 61[e] | 0.18 | 99 ± 13 | 98.7 |
| 2t | 115[e] | 0.28 | 83 ± 7 | 80.1 |
| 3t | 245[e] | 0.49 | 61.5 ± 6 | 62.2 |
| 4t | 460[e] | 0.90 | 50 ± 4.5 | 50.5 |
| 5t | 920[f] | 1.80 | 38 ± 2 | 36.2 |
| 6t | 1520[f] | 2.95 | 30.3 ± 0.9 | 28.1 |
| 7t | 4430[f] | 8.95 | 18.5 ± 0.7 | 16.5 |
| Experiments with Silica Surface and Titania Colloid | | | | |
| 1st | 61[e] | 0.18 | 92 ± 11 | 98.7 |
| 2st | 115[e] | 0.24 | 82 ± 7 | 80.1 |
| 3st | 245[e] | 0.49 | 62 ± 7 | 62.2 |
| 4st | 454[e] | 0.88 | 50.4 ± 4.9 | 50.6 |
| 5st | 918[f] | 1.75 | 37.3 ± 3.9 | 36.2 |
| 6st | 1520[f] | 2.95 | 29.6 ± 1.4 | 28.1 |
| 7st | 4425[f] | 8.97 | 18.1 ± 0.9 | 16.5 |
| 8st | 8590[f] | 18.6 | 13.3 ± 0.9 | 11.8 |

[a] Concentration of KPAA expressed in ppm on wt/wt basis. [b] Suspension ionic strength obtained from the conductivity measurements. [c] The period of structural oscillations in the experimental force profile. The reported variability represents standard deviation whenever more than 4 measurements were available. [d] For the dilute polyelectrolyte solution regime, $\xi_{bulk}$ represents the predicted macromolecule−macromolecule spacing in the bulk (i.e., $\xi_{bulk} = R_{cm}$) and was calculated according to eq 5. In the semidilute regime, $\xi_{bulk}$ denotes the bulk correlation length and was computed from eq 8. [e] Corresponds to the dilute polyelectrolyte solution regime ($c < c^*$, where $c^* = 502$ ppm). [f] Corresponds to the semidilute polyelectrolyte solution regime ($c > c^*$, where $c^* = 502$ ppm). [g] No structural oscillations were detected in the measured force profile.

onset was phenomenologically found to occur when each chain overlapped with $p$ others,[48−50] where $p$ was in the range 5−10, depending on the polymer investigated. Applying the same criterion to the salt-free polyelectrolyte solutions yields[45]

$$n_e = p^4 n^* \text{ and } 5 \le p \le 10 \qquad (10)$$

where $n_e$ denotes the monomer number concentration at which entanglement begins and $n^*$ is the overlap concentration defined earlier.

The relevant parameters for the polyacrylate chains used in these experiments (i.e., KPAA or NaPAA at pH greater than the polyacid p$K_a$) are: $b$(monomer size) = 0.3 nm, $l_B$(Bjerrum length) = 0.7 nm, $N$ (average number of monomers per chain) = 322, and $A$(number of monomers between charges) = 5.[45,51,52] Substituting these values into the above equations yields $L$ = 49.0 nm, $n^* = 2.8 \times 10^{18}$ monomers/cm$^3$ (or $c^* = 502$ ppm by weight), and $n_e = 1.9 \times 10^{21}$ monomers/cm$^3$ (or $c_e = 3.1 \times 10^5$ ppm by weight).

*Experimental Data vs Scaling Theory.* To compare the experimental measurements to theory, the bulk spacing between polyelectrolyte macromolecules ($\xi_{bulk} = R_{cm}$) was calculated in the dilute solution regime ($c < 502$ ppm) using eq 5. Similarly, eq 8 was employed to determine the bulk correlation length ($\xi_{bulk}$) in the semidilute regime ($c > 502$ ppm). These predicted $\xi_{bulk}$ values for both solution regimes are reported in Table 2, together with experimentally measured $\xi_{exp}$. Furthermore, Figure 7 shows the comparison between $\xi_{exp}$ (symbols) and $\xi_{bulk}$ (line) for all the experiments listed in Table 2. The data are plotted as a function of KPAA concentration with the condition for overlap (i.e., $c^* = 502$ ppm) also indicated in the graph. Note the since eqs 7 and 8 are scaling relationships (i.e., each contains an unknown numerical prefactor), the value of the predicted correlation length in the semidilute regime was matched to the dilute prediction at $c = c^*$. As can be seen from this figure, the quantitative agreement is excellent in the dilute regime (i.e., the average error is 1.7% for the $c < 502$ ppm measurements reported in Table 2 with the largest deviation not exceeding 7%). In addition, the experimental data follows a scaling law of the form $\xi_{exp} \sim c^{-0.32\pm0.01}$, consistent with a space-filling behavior.

In the semidilute regime, quantitative comparison is more difficult due to the limited number of measurements available. Particularly, the wavelength of the oscillations in the measured force profiles could not be determined at concentrations greater than approximately 4430 ppm, possibly due to the formation of adsorbed polyelectrolyte layers. Nonetheless, as shown in Table 2, the $\xi_{exp}$ values are 7.4% larger than $\xi_{bullk}$ on average, with the largest deviation not exceeding 13%, and follow the same scaling with respect to bulk KPAA concentration. Specifically, $\xi_{exp} \sim c^{-0.47\pm0.01}$ was found experimentally and $\xi_{bulk} \sim c^{-1/2}$ is expected of the bulk solution. Thus as was the case with the charged nanospheres, the structure of the polyelectrolytes in the gap region matches that of the bulk solution.

Similar conclusions were reached by Langevin and coworkers[38−40] investigating the stepwise draining of thin films containing semidilute polyelectrolyte/surfactant mixtures. The observed pressure oscillations, which are analogous to the force oscillations reported in the current study, were related to a network of polyelectolyte coils in the bulk. Particularly, the wavelength of these oscillations scaled as $\sim c^{-0.5}$ and its absolute value compared well with the predicted correlation length of the bulk polyelectrolyte network for the concentration range investigated.

The bulk behavior of NaPAA chains ($M_w$ = 33000 and 99000 g/mol, $M_w/M_n \le 1.15$) confined between silica surfaces was also reported by Milling and Kendall.[17] Almost all of their AFM measurements were performed in the semidilute regime and $\xi_{exp} \sim c^{-0.5}$ was found. Similar scaling behavior (i.e., $\xi_{exp} \sim c^{-0.48}$) was reported in an earlier study by Milling[16] with NaPSS polyelectrolyte ($M_w$ = 46100 and 200000 g/mol, $M_w/M_n < 1.1$) between silica surfaces. These results are quite interesting, because while the larger polymer was in the semidilute regime, the smaller polymer ($M_w$ = 46100) was actually in the dilute regime where $\xi \sim c^{-1/3}$ bulk scaling is expected. This was found not to be the case (i.e., as mentioned above, $\xi_{exp} \sim c^{-0.48}$ was determined instead) and Milling and Kendall attributed the observed behavior to the electrostatic nature of the chain-chain interactions (i.e., the bulk electrostatic screening length, which scales as $\sim c^{-1/2}$, would control the spacing of the polymer chains in the gap region).

In a more recent TIRM study, Biggs et al.[15] have shown that NaPSS coils ($M_w \approx$ 35000 g/mol, $M_w/M_n$ = 1.01) in dilute regime are space-filling at sufficiently large gap widths between the two surfaces employed (i.e., borosilicate glass sphere and a silica substrate). Specifically, the oscillation wavelength in the measured potential energy profiles[53] followed a $\xi_{exp} \sim c^{-0.35}$ scaling law. Interestingly, however, at higher concentrations (still in the dilute regime though), the inner oscillations located at

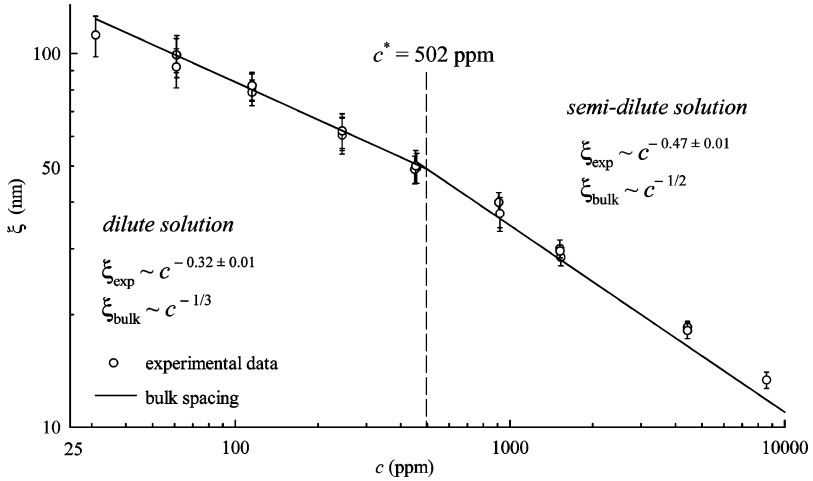


**Figure 7.** Graph illustrating the experimentally observed scaling behavior of KPAA chains between two surfaces and the bulk polyelectrolyte behavior predicted by the scaling theory. The period of force oscillations in the measured force profiles ($\xi_{exp}$) is denoted by open circles, with vertical error bars representing the measurement standard deviation. These data correspond to experiments listed in Table 2 for which $\xi_{exp}$ could be reliably determined. The solid lines correspond to predictions of eq 5 in the dilute regime and eq 8 in the semidilute regime for the bulk polyelectrolyte solution. Moreover, the overlap concentration ($c^*$) calculated from eq 6 is also indicated. The value of the predicted correlation length in the semidilute regime was matched to the dilute prediction at $c = c^*$.

smaller gap widths scaled as $\xi_{exp} \sim c^{-0.56}$. This was explained as ordering of the confined polyelectrolyte chains parallel to the interface (i.e., a closed packed system of parallel rods should scale as $\xi \sim c^{-1/2}$). (This suggestion that the chains align parallel to the confining surfaces is supported by the Monte Carlo simulations of Jönsson et al.[37])The scaling exponents of $-0.35$ and $-0.56$ for the "bulk" and "confined" polymers, respectively, should be compared with the value of $-0.48$ obtained by Milling (see above). It is hypothesized here that the $\xi_{exp} \sim c^{-0.48}$ scaling relation found in Milling's study for dilute solutions of 46100 g/mol NaPSS might be attributed to chain confinement effects analogous to those reported by Biggs and co-workers (i.e., a structure of parallel rods aligned parallel to the interface).

In the present study, both the inner and the outer structural oscillations scaled similarly with KPAA concentration according to the $\xi_{exp} \sim c^{-0.32}$ scaling law in the dilute polyelectrolyte solution regime (i.e., $c < 502$ ppm). This may point to a different behavior under confinement for the more hydrophobic NaPSS chains as compared to the KPAA polyelectrolyte, which has a more hydrophilic backbone.

Finally, a comment should be made about the accuracy of the predicted overlap concentration, $c^*$. As seen in Figure 7, this predicted value appears to mark relatively accurately the boundary between the two different scaling regimes observed in the force profiles. Clearly this is somewhat fortuitous, as the value of $c^*$ was calculated using the average degree of polymerization of the chains and ignoring polydispersity. Because of the long tail at high molecular weights shown in Figure 1, it seems likely this polydispersity would tend to greatly lower the true value of $c^*$. However, it should also be mentioned that the calculation procedure assumed a perfectly rodlike polymer conformation, and deviations from this shape would seemingly tend to increase the overlap concentration. Thus these two effects would tend to cancel each other.

## Conclusions

The primary finding from this study was that the structure of the nonadsorbing material in the gap region was essentially the same as that predicted for the bulk. For the case when the nonadsorbing material was simple charged nanospheres, the wavelength of structural oscillations in the force profile scaled as the bulk polymer concentration, $c$, as $c^{-1/3}$. In addition, the actual magnitude of this wavelength could be accurately predicted using the simple expression $\xi = n^{-1/3}$, where $n$ is the bulk number density.

This simple expression was also found to work in polyelectrolyte systems when the bulk polymer concentration was below the overlap concentration. Above the overlap concentration, the wavelength was found to scale as $c^{-1/2}$, which is the scaling expected for the characteristic mesh size in the semidilute regime.

This finding that the wavelength of the oscillations matched the predicted bulk spacing was somewhat unexpected, as the conditions in the gap region are assumed to be different from those in the bulk (otherwise, there would be no net interaction force between the particle and substrate). It is possible that at the relatively large separation distances used in determining these wavelengths (i.e., much larger than the bulk Debye length of the system), the conditions in the gap region remain similar to those in the bulk. Clearly this behavior needs to be investigated more fully, and additional modeling work in this area is currently underway. Nonetheless, these experiments do provide a relatively simple method for determining the bulk structure of these complex systems.

**Acknowledgment.** The authors thank Nicolay Tsarevsky and Professor Krzysztof Matyjaszewski from the Department of Chemistry at Carnegie Mellon University for their assistance in characterizing the potassium polyacrylate polymer, and to Ms. Stephanie Eiden at the University of Konstanz for synthesizing the $TiO_2$ particles. Support for this work was provided by the National Science Foundation under Grant CTS-9912098 and by Millennium Inorganic Chemicals.

## References and Notes

(1) Evans, R.; Henderson, J. R.; Hoyle, D. C.; Parry, A. O.; Sabeur, Z. A. *Mol. Phys.* **1993**, *80*, 755.
(2) Vlachy, V. *Langmuir* **1996**, *121*, 2881.
(3) Gotzelmann, B.; Evans, R.; Dietrich, S. *Phys. Rev. E* **1998**, *57*, 6785.
(4) Lutterbach, N.; Versmold, H.; Reus, V.; Belloni, L.; Zemb, Th. *Langmuir* **1999**, *15*, 337.
(5) Lutterbach, N.; Versmold, H.; Reus, V.; Belloni, L.; Zemb, Th.; Lindner, P. *Langmuir* **1999**, *15*, 345.
(6) Louis, A. A.; Allahyarov, E.; Lowen, H.; Roth, R. *Phys. Rev. E* **2002**, *65*, 061407.
(7) Basheva, E. S.; Nikolov, A. D.; Kralchevsky, P. A.; Ivanov, I. B.; Wasan, D. T. *Proc. Int. Symp.* **1991**, *11*, 467.

(8) Nikolov, A. D.; Wasan, D. T. *Langmuir* **1992**, *8*, 2985.
(9) Wasan, D. T.; Nikolov, A. D.; Kralchevsky, P. A.; Ivanov, I. B. *Colloids Surf.* **1992**, *267*, 139.
(10) Wasan, D. T.; Nikolov, A. D. In *Particulate Two Phase Flow*; Roco, M. C., Ed.; Bethernorth-Heinemann: New York 1993; p 325.
(11) Sober, D. L.; Walz, J. Y. *Langmuir* **1995**, *11*, 2352.
(12) Sharma, A.; Walz, J. Y. *J. Chem. Soc., Faraday Trans.***1996**, *92*, 4997.
(13) Sharma, A., Ph.D. Thesis, *Prediction and Measurement of the Depletion Interaction in Charged Colloidal Systems and its Effect on Stability*, Tulane University, 1997.
(14) Sharma, A.; Tan, S. N.; Walz, J. Y. *J. Colloid Interface Sci.* **1997**, *191*, 236.
(15) Biggs, S.; Dagastine, R. R.; Prieve, D. C. *J. Phys. Chem. B* **2002**, *106*, 11557.
(16) Milling, A. J. *J. Phys. Chem.* **1996**, *100*, 8986.
(17) Milling, A. J.; Kendall, K. *Langmuir* **2000**, *16*, 5106.
(18) Burns, J. L.; Yan, Y.; Jameson, J.; Biggs, S. *Colloids Surf. A* **2000**, *162*, 265.
(19) Biggs, S.; Burns, J. L.; Yan, Y.; Jameson, J.; Jenkins, P. *Langmuir* **2000**, *16*, 9242.
(20) Burns, J. L.; Yan, Y.; Jameson, J.; Biggs, S. *J. Colloid Interface Sci.* **2002**, *247*, 24.
(21) Piech, M.; Walz, J. Y. *J. Colloid Interface Sci.* **2002**, *253*, 117.
(22) Richetti, R.; Kekicheff, P. *Phys. Rev. Lett.* **1992**, *68*, 1951.
(23) Crocker, J. C.; Matteo, J. A.; Dinsmore, A. D.; Yodh, A. G. *Phys. Rev. Lett.* **1999**, *82*, 4352.
(24) Eiden, S.; Maret, G. *J. Colloid Interface Sci.* **2002**, *250*, 281.
(25) O'Brien, R. W.; White, L. R. *J. Chem. Soc., Faraday Trans. 2* **1978**, *74*, 1607.
(26) Walker, S. L.; Bhattacharjee, S.; Hoek, E. M. V.; Elimelech, M. *Langmuir* **2002**, *18*, 2193.
(27) Van Blaaderen, A.; Kentgens, A. P. M. *J. Non-Cryst. Solids* **1992**, *149*, 161.
(28) Pusey, P. N.; Fijnaut, H. N.; Vrij, A. *J. Chem. Phys.* **1982**, *77*, 4270.
(29) Ducker, W. A.; Senden, T. J. Pashley, R. M. *Langmuir* **1992**, *8*, 1831.
(30) Sader, J. E.; Chon, J. W. M.; Mulvaney, P. *Rev. Sci. Instrum.* **1999**, *70*, 3967.
(31) Chan, D. Y. C.; Horn, R. G. *J. Chem. Phys.* **1985**, *83*, 5311.
(32) Sader, J. E.; Larson, I.; Mulvaney, P.; White, L. R. *Rev. Sci. Instrum.* **1995**, *66*, 3789.
(33) Laven, J.; Stein, N. *J. Colloid Interface Sci*. **2001**, *238*, 8.
(34) Finsy, R.; Moreels, E.; Bottger, A.; Lekkerkerker, H. *J. Chem. Phys.* **1985**, *82*, 3812.
(35) Dezelic, G.; Kratohvil, J. P. *Kolloid Z.* **1960**, *173*, 38.
(36) Honig, E. P.; Punt, W. F. J.; Offermans, P. H. G. *J. Colloid Interface Sci*. **1990**, *134*, 169.
(37) Jönsson, B.; Broukhno, A.; Forsman, J.; Åkesson, T. *Langmuir* **2003**, *19*, 9914.
(38) Bergeron, V.; Langevin, D.; Asnacios, A. *Langmuir* **1996**, *12*, 1550.
(39) Asnacios, A.; Espert, A.; Colin, A.; Langevin, D. *Phys. Rev. Lett.* **1997**, *78*, 4974.
(40) Klitzing, R. V.; Espert, A.; Asnacios, A.; Hellweg, T.; Colin, A.; Langevin, D. *Colloids Surf. A* **1999**, *149*, 131.
(41) Odjik, T. *J. Polym. Sci., Polym. Phys. Ed.* **1977**, *15*, 477.
(42) Skolnick, J.; Fixman, M. *Macromolecules* **1977**, *10*, 944.
(43) Stevens, M.; Kremer, J. *Phys. Rev. Lett.* **1993**, *71*, 2228.
(44) Stevens, M.; Kremer, J. *J. Chem. Phys.* **1995**, *103*, 1669.
(45) Dobrynin, A. V.; Colby, R. H.; Rubinstein, M. *Macromolecules* **1995**, *28*, 1859.
(46) Bjerrum, N. *Z. Electrochem.* **1918**, *24*, 321.
(47) de Gennes, P.-G. *Scaling Concepts in Polymer Physics*; Cornell University Press: Ithaca, NY, 1979.
(48) Kavassalis, T. A.; Noolandi, J. *Phys. Rev. Lett.* **1987**, *59*, 2674.
(49) Kavassalis, T. A.; Noolandi, J. *Macromolecules* **1989**, *22*, 2709.
(50) Lin, Y.-H. *Macromolecules* **1987**, *20*, 3080.
(51) Konop, A. J.; Colby, R. H. *Macromolecules* **1999**, *32*, 2803.
(52) Weill, C.; Lachhab, T. Moucherout, P. *J. Phys. II (France)* **1993**, *3*, 927.
(53) Total internal reflection microscopy (TIRM) determines the potential profile for the interaction between a Brownian colloid and a flat surface. Because interaction potential and force are simply related (i.e., force is the negative gradient of the potential), the wavelength of the oscillations in the corresponding potential and force profiles is the same.